Electronic band structure of single-crystal and single-layer WS_2: Influence of interlayer van der Waals interactions

A. Klein,[1] S. Tiefenbacher,[2] V. Eyert,[3] C. Pettenkofer,[2] and W. Jaegermann[1]
[1]*Darmstadt University of Technology, Institute of Materials Science, Petersenstrasse 23, D-64287 Darmstadt, Germany*
[2]*Hahn-Meitner-Institut, Solar Energy Division, Glienicker Strasse 100, D-14109 Berlin, Germany*
[3]*University of Augsburg, Institute of Physics, D-86135 Augsburg, Germany*
(Received 19 February 2001; revised manuscript received 2 July 2001; published 2 November 2001)

The valence band structure of the layered transition metal dichalcogenide WS_2 has been determined experimentally by angle resolved photoelectron spectroscopy and theoretically by augmented spherical wave band structure calculations as based on density functional theory. Good agreement between experimental and calculated band structure is observed for single crystal WS_2. An experimental band structure of a single layer was determined from an electronically decoupled film prepared on a single crystalline graphite substrate by metal-organic van der Waals epitaxy. The polarization dependent photoemission selection rules of the single layer film are appropriate for a free standing film. The experimental single layer band structure shows some differences compared to band structure calculations using bulk atomic positions within the layer. We conclude that relaxation of the single layer occurs as a consequence of the missing interlayer interactions leading to close agreement between electronic structure of the single layer and single crystal. As a consequence of the missing interlayer interactions the valence band maximum for the single layer is located at the *K* point of the Brillouin zone.

DOI: 10.1103/PhysRevB.64.205416 PACS number(s): 73.21.−b, 71.20.Nr, 79.60.Jv

I. INTRODUCTION

The electronic structure of semiconducting layered chalcogenides has been studied for decades both theoretically [1–13] and experimentally[11–20] because of their interesting quasi-two-dimensional crystallographic structure. Recent review on electron spectroscopical studies of these materials are given in Ref. 19. Strong covalent chemical bonds are present inside the layers while the interactions between the layers are usually described as van der Waals–like. As a result there is strong dispersion of the energy bands parallel to the layers while only small dispersion is observed perpendicular to the layers.

Interlayer interactions are of particular importance for the layered materials since they are responsible for the anisotropy of their physical and chemical properties. Any application involving heterointerfaces between different layered materials depends on the electronic coupling across the van der Waals gap. Such interfaces can be prepared by van der Waals epitaxy on different two-dimensional as well as three-dimensional (e.g., Si, GaAs) substrates.[21,22] A variety of atoms or molecules are known to intercalate into the van der Waals gap of layered chalcogenides modifying the interlayer interaction.[23–25] Also the preparation of fullerenelike and nanotube materials of such compounds has been achieved recently.[26,27] A better understanding of the electronic structure of layered compounds in dependence on the arrangement of the layers, which determine the interlayer interactions, is thus highly demanded.

WS_2 and its isoelectronic compounds WSe_2, $MoSe_2$, and MoS_2 are semiconductors with bandgaps between 1 and 1.5 eV[28]. To our knowledge the only published calculation of the electronic structure of WS_2 is the semiempirical tight binding calculation of Bromley *et al.*[7] Very recently a band structure calculation has been performed by Seifert *et al.* for single-wall WS_2 nanotubes.[6] In contrast to WS_2, a number of band structure calculations exist for WSe_2, $MoSe_2$, or MoS_2.[7–13] Since these are isolectronic to WS_2 they can be expected to have very similar electronic structures. There are also several experimental determinations of the electronic band structure of WSe_2,[11–13] $MoSe_2$,[11,17] MoS_2,[11,14,15,17] and $MoTe_2$ (Refs. 17,18) using angle-resolved ultraviolet photoelectron spectroscopy. No experimental band structure of WS_2 has been published so far.

In the 1960's and 1970's a number of authors have calculated two-dimensional electronic structure of layered materials such as, e.g., single layer GaSe (Refs. 3) or single layer transition metal dichalcogenides.[7,9] Using density functional theory a calculation of three- and two-dimensional (single layer) band structures for MoS_2 has been presented by Kobayashi and Yamauchi in order to understand scanning tunneling microscopy images of transition metal dichalcogenide surfaces.[10] A MoS_2 single crystal band structure was calculated using a plane wave basis set. In comparison a single layer band structure was calculated using a LCAO (linear combination of atomic orbitals) wave function basis. The band structures calculated for single crystal and single layer are very similar. The differences, which are present, e.g., for the overall valence band width, most likely traced back to the different calculation method used, because very similar differences are observed for slabs of four layer thickness, where results for both basis sets are presented by the authors.[29]

A crucial point in calculations of isolated slabs of layered materials is the assumption of their crystallographic structure. There exist crystallographic data on *exfoliated* single layer MoS_2 and WS_2.[30,31] In this approach single layers are produced from single crystals by intercalation of Li into the van der Waals gap and subsequent dissolution in water. Dis-

solution of the chalcogenides in water as single layers occurs only after intercalation with a considerable amount of Li. Intercalation, however, leads to a structural phase transformation from the $2H$ to the $1T$ modification accompanied by an increase of the *a* lattice constant as determined from x-ray diffraction.[30,31] An intercalation induced phase transition has already been described previously in the literature[32] and has also been suggested from photoemission studies of Li intercalated WS_2 (Ref. 33) and MoS_2 (Ref. 34) single crystals. These exhibit clear changes of the electronic structure with increasing Li content.[33,34] Hence the existing structural data correspond to the $1T$ modification of MoS_2 or WS_2 and can therefore not be used to determine the atomic positions of trigonal prismatically coordinated Mo or W dichalcogenides.

Because of the lack of experimental data on single layer trigonal prismatic coordinated WS_2 Kobayashi and Yamauchi have assumed identical atomic positions within the layers for any of the structures in the calculations.[10] This procedure is not justified as the lattice constants may be significantly different because of the missing interlayer interactions. However, the same approach has been used by Fang *et al.*[4] They calculated the electronic structure of bulk TiS_2 and $TiSe_2$, as well as of TiS_2 and $TiSe_2$ slabs with different number of layers. In their calculation single crystal TiS_2 and $TiSe_2$ are found to be semimetallic while a single slab of TiS_2 with identical atomic positions compared to the bulk crystal structure is a semiconductor.[4] This shows that a major electronic property of these material can depend on interlayer interactions. However, it is noted that there is no general agreement in the literature about the semimetallic nature of bulk TiS_2.[5,35] In any case, the experimental test of such theoretical predictions would require the determination of the electronic structure of isolated single layer material.

In contrast to atoms, molecules or small clusters the experimental determination of the electronic structure of extended two-dimensional single layers of atomic thickness requires the deposition onto a suitable substrate. Sufficient crystalline quality is thereby generally achieved by the strong interaction with a crystalline substrate, which, unfortunately, also modifies the crystallographic and electronic structure of the layer. In the case of layered chalcogenides, it is possible to prepare epitaxial films on van der Waals–terminated surfaces without the constraint of lattice matching.[21,22] When films are deposited onto substrates with strongly different electronic structure the electronic states of the film cannot couple with the substrate. This has been shown experimentally for InSe films deposited on highly oriented pyrolytic graphite (HOPG).[36] Such an electronically decoupled layer can be considered as a free-standing film in the sense of its electronic properties. In order to determine the dispersion of the energy bands along the layers single crystalline films are required, which can only be prepared on single crystalline substrates and not on HOPG. An experimental determination of the electronic structure of single layer HfS_2 deposited on a single crystal WSe_2 substrate has been presented by Kreis *et al.*[37] Single layer thickness is confirmed by *in situ* scanning tunneling microscopy on the same samples. However, the **k**-resolved dispersion of individual electronic bands could only partly be determined for this system because of intense substrate emissions. The lack of significant electronic substrate/film interactions has also not been shown explicitly.

In this work we describe the experimental determination of the electronic valence band structure of single layer WS_2 by angle-resolved photoelectron spectroscopy using synchrotron radiation as excitation source. The films were prepared by metal-organic van der Waals-epitaxy on single crystalline graphite substrates.[38–40] We will further present an experimental determination of the valence band structure of single crystal WS_2 and theoretical band structure calculations based on density functional theory for both single layer and single crystal.

The paper is organized as follows. In Sec. II the crystallographic structures of single crystal and single layer WS_2 are presented. We will also show symmetrized orbital combinations at the Γ point of the Brillouin zone for the space groups of both structures. In Sec. III the method and results of band structure calculations are described together with a discussion of the observed differences for single crystal and single layer. The experimental setup is outlined in Sec. IV A. Experimental results and a comparison with theory for the single crystal are presented in Sec. IV B. Section IV C is dedicated to thin film preparation and to the experimental band structure of the single layer, which is discussed in relation with theory and with the single crystal band structure. For this purpose we have evaluated polarization dependent photoemission selection rules along the Σ symmetry line. Finally the results and conclusions are summarized in Sec. V.

II. CRYSTALLOGRAPHIC STRUCTURE AND ORBITAL SYMMETRY

WS_2 belongs to the layered transition metal dichalcogenides, which crystallize in a two-dimensional structure composed of covalently bonded *X-M-X* sandwiches (X=S, Se; M=Mo,W,Ta,Nb,V,Ti,Zr,Hf).[1] There is only weak interaction across the layers generally referred to as van der Waals–like. The crystal lattice of the $2H$ polytype of WS_2 belongs to the nonsymmorphic hexagonal space group $P6_3/mmc$ (D_{6h}^4). In the $2H$ polytype the unit cell is extended over two layers with the S atoms of the second layer on top of the W atoms of the first layer and vice versa. The W atoms are in a trigonal prismatic coordination. Lattice constants are given by Schutte *et al.* as $a=3.153$ Å and $c=12.323$ Å.[41] The *z*-parameter, determining the relative positions of the sulfur atoms along z is given by 0.6225. The crystallographic structure is shown in Fig. 1 together with the hexagonal Brillouin zone.

A single layer of WS_2 is composed of one S-W-S stacking unit. It has a threefold rotational axis (c axis). The plane containing the W atoms is a mirror plane. As a result of this mirror plane the symmetry properties of the single layer can not be described by one of the two-dimensional space groups but rather by the three-dimensional space group $P\bar{6}m2$ (D_{3h}^1). Compared to $P\bar{6}m2$ the space group $P6_3/mmc$ of the single crystal has the inversion as additional symmetry operation.

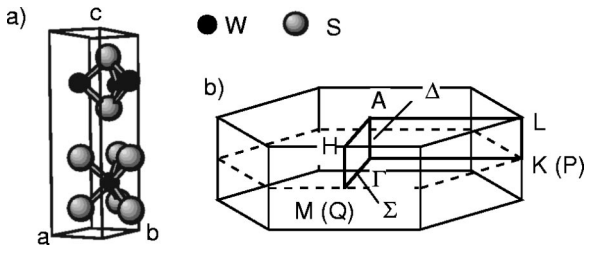

FIG. 1. Crystal structure (a) and Brillouin zone (b) of $2H$-WS_2. The labels given in brackets for some of the high symmetry points in the Brillouin zone are sometimes used for two-dimensional systems.

The high symmetry points at the Brillouin zone boundary for two-dimensional hexagonal materials are usually labeled as Q and P. For convenience we use throughout this paper the same labels as for the single crystal where $M(K)$ corresponds to $Q(P)$ (see Fig. 1). Symmetrized combinations of valence orbitals belonging to the irreducible representations are given in the literature for both space groups.[3,7,9,42] Electronic states being symmetric (antisymmetric) with respect to reflection at the horizontal mirror plane of the single layer were labeled in this work with superscripts $+(-)$, respectively, instead of the sometimes used primed and unprimed symbols. Electronic states of the single crystal labeled with superscripts $+(-)$ are symmetric (antisymmetric) with respect to inversion. A view of symmetrized combinations of sulfur p_x and p_z orbitals at Γ are shown in Fig. 2. At Γ the states derived from p_x and p_y orbitals are degenerate.

The four different combinations for each orbital can be classified into bonding and antibonding states with respect to intralayer and interlayer interactions along the crystallographic c direction. For the p_z orbitals the intralayer interaction is σ-like and gives rise to a strong bonding/antibonding splitting. The two intralayer bonding states are Γ_1^+ and Γ_4^-.

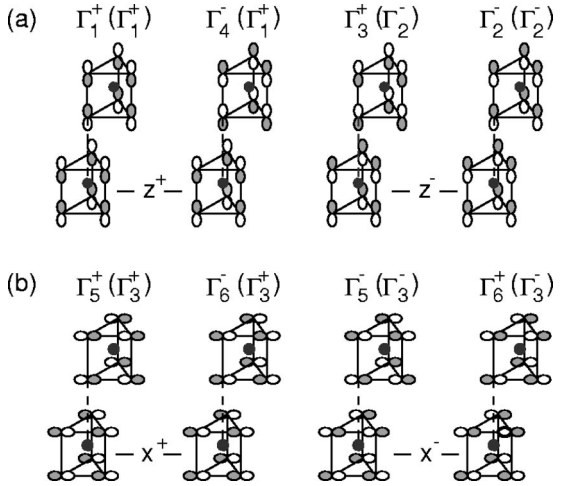

FIG. 2. Possible combinations of p_z (a) and p_x (b) orbitals in a WS_2 unit cell with symmetry labels used for the irreducible representations of the $P6_3/mmc$ space group (Refs. 9,42). Combinations of single layer states are obtained by omitting the second layer. Symmetry labels for single layer states as used in this paper are given in brackets.

Interlayer bonding states of the p_z orbitals are Γ_1^+ and Γ_3^+.

The intralayer interactions of the p_x and p_y orbitals along c are π-like resulting in a weaker splitting of the resulting energy states of about 1.2 eV (see Sec. III). The interlayer interactions of the states derived from p_x and p_y orbitals are generally very weak. A small energy splitting of 0.1 eV is observed between Γ_5^- and Γ_6^+. Almost no splitting is observed between Γ_5^+ and Γ_6^- (see Fig. 2 and Sec. III).

In the transition metal dichalcogenides there is pronounced hybridization between the chalcogenide p orbitals and the metal d orbitals.[9,7] Hybridization between p_z and d_{z^2} at Γ forms the electronic states at the valence band maximum in many of those compounds[11]. The Γ_5^+ and Γ_6^- states mix with the d_{xy} and $d_{x^2-y^2}$ orbitals, while the Γ_5^- and Γ_6^+ states mix with d_{xz} and d_{yz} orbitals. We will use the terms x^+ and x^- in this article for the corresponding energy states, where the superscript indicates the intralayer interaction (see also Fig. 2). In accordance with this convention the 1^+ and 4^- combinations of the p_z orbitals at Γ are referred to as z^+ and the 3^+ and 2^- combinations as z^-.

III. BAND STRUCTURE CALCULATIONS

A. Single crystal WS_2

The band structure calculations are based on density functional theory (DFT) and the local density approximation (LDA).[43,44] We employ the augmented spherical wave (ASW) method[45] in its scalar-relativistic implementation (see Refs. 46–48 for more recent descriptions). Since the ASW method uses the atomic sphere approximation (ASA),[49] we had to insert so-called empty spheres into the open crystal structure of $2H$-WS_2. These empty spheres are used to model the correct shape of the crystal potential in large voids. In order to minimize the sphere overlap, we have recently developed an algorithm,[50] which solves the problem of finding optimal empty sphere positions as well as radii of all spheres automatically. By inserting six empty spheres into the hexagonal unit cell of $2H$-WS_2 we kept the linear overlap of any two physical spheres below 11%, and the overlap of any pair of physical and empty spheres below 22%.

The Brillouin zone sampling was done using an increased number of **k** points ranging from 36 to 576 points within the irreducible wedge of the hexagonal Brillouin zone. This way we were able to ensure convergence of our results with respect to the fineness of the **k**-space grid. Self-consistency was achieved by employing an efficient algorithm for convergence acceleration.[51] Convergence criteria for the atomic charges and the total energy were 10^{-8} electrons and 10^{-8} Ryd, respectively.

In Fig. 3 we show the calculated band structure of single crystal WS_2. As for its isoelectronic compounds WSe_2, MoS_2, and $MoSe_2$,[11–13] the calculation reveals that WS_2 is an indirect semiconductor with the valence band maximum at the center of the Brillouin zone. The conduction band minimum lies between Γ and K with a bandgap of $E_g \approx 1.2$ eV, close to the experimental value of 1.34 eV.[28] There are 14 filled bands in the Brillouin zone. The 28 electrons per unit cell are supplied by 2×4 electrons from W $5d$, 2×2

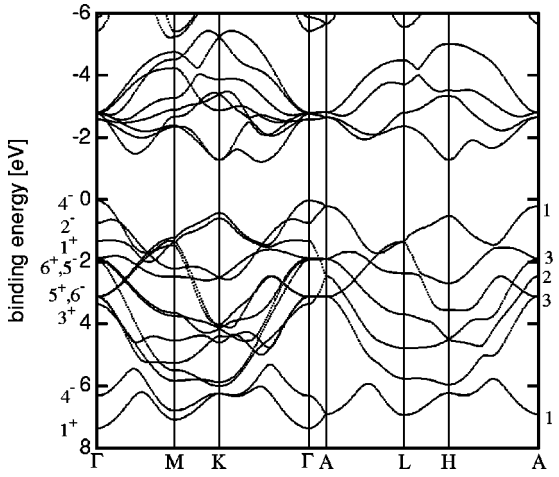

FIG. 3. Band structure of single crystal WS_2 calculated using the augmented sperical wave method. The zero of binding energy corresponds to the position of the valence band maximum. Symmetry labels for Γ (A) of the corresponding valence states are indicated at the left (right) axis of the graph.

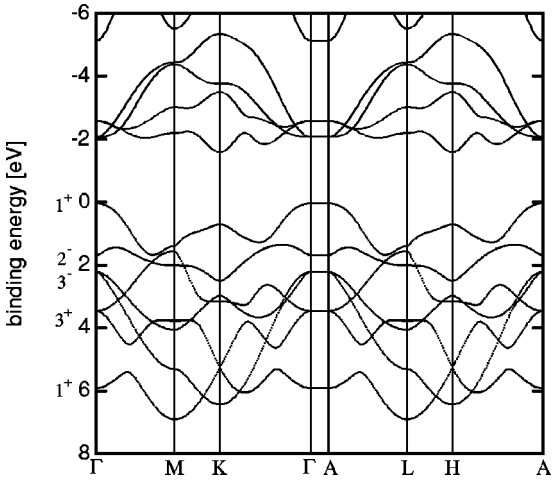

FIG. 4. Band structure of single layer WS_2 calculated using the augmented sperical wave method. The zero of energy corresponds to the energetic position of the valence band maximum. Symmetry labels for the center of the Brillouin zone Γ are indicated at the left axis.

electrons from W $6s$, and 4×4 electrons from S $3p$ orbitals. The S $3s$ electrons, which have also been included in the calculation, form separate bands which are outside the energy window in Fig. 3.

In the top plane of the Brillouin zone (A-L-H) there is generally a double degeneracy of each band.[9] The interactions across the van der Waals–plane are evident from the lift of degeneracy when going from A to Γ. There are three pairs of occupied bands which show considerable splitting at Γ and are degenerate at A. The corresponding energy bands are mainly derived from $5d_{z^2}$ orbitals with a binding energy of 0.21 eV at A, and from $3p_z$ orbitals at 2.46 and 6.90 eV, respectively. The strong difference of 4.44 eV between the binding energies of the two $3p_z$ bands at A is due to the intralayer bonding/antibonding splitting (see Fig. 2). The splitting of each of these three bands at Γ is due to the interlayer bonding/antibonding combinations. With increasing binding energy the three topmost filled valence states at Γ are the 4^-, 2^-, and 1^+ states. This order indicates an overlap between the S $3p$ (2^-) and W $5d$ (1^+,4^-) states.

The A_3 bands at binding energies of 3.12 and 1.91 eV at A show almost no splitting at Γ and no dispersion along ΓA. They are derived from the S $3p_x$ (p_y) orbitals. The energy difference of 1.21 eV corresponds to the intralayer bonding/antibonding splitting between the x^+ (Γ_5^+ and Γ_6^-) and x^- (Γ_5^- and Γ_6^+) states (see Fig. 2). Each of these states is still doubly degenerate at Γ. A small splitting of less than 0.1 eV between the pairs of the 5^- and 6^+ states is present at Γ as already mentioned in Sec. II. In principle the 5^+,6^- and 5^-,6^+ states should split into two pairs of bands due to spin-orbit coupling, which is not included in our calculation.

B. Single layer WS_2

A unit cell for the calculation of the single layer band structure was constructed by replacing all atoms of the second layer in the single crystal unit cell by empty spheres. The atomic positions in the single layer are thus assumed to be identical to the single crystal as also done in the literature.[4,10] Subsequent layers are consequently separated by one sandwich unit. The dimensions of the Brillouin zone are identical to those of the single crystal because of the same size of the unit cell used in the calculation. Due to the loss of the full symmetry of the 2H structure in our supercell calculations the Brillouin zone sampling included 63 to 1088 **k** points within the irreducible wedge.

The calculated band structure is shown in Fig. 4. Any remaining interactions perpendicular to the layers are found to be small. This is indicated by the lack of binding energy dispersion for all bands along ΓA and from the identical band structures in the Γ-M-K and the A-L-H planes. According to Fig. 4 single layer WS_2 is a (two-dimensional) semiconductor with the valence band maximum at Γ. The conduction band minimum is at the K point of the Brillouin zone at a binding energy of -1.6 eV, which corresponds to the calculated energy gap of the single layer. In contrast to the single crystal band structure there are only seven filled bands below the Fermi energy because the unit cell extends over one sandwich layer and contains only one W and two S atoms.

The overall appearance of the single layer band structure is very similar to the single crystal band structure as can be expected from the small interlayer interactions in layered compounds and as also observed for band structure calculations of other materials.[4,9,10] However, some differences in the dispersion of the bands are particularly observed around the K/H points. These can be attributed to different hyridization as a result of different crystal symmetries of the two structures (see Sec. II).

Binding energies corresponding to the $5d_{z^2}$ and to the $3p_z$ orbitals at Γ are 0, 1.69, and 5.91 eV, respectively. The intralayer bonding/antibonding splitting of p_z at Γ is hence 4.22 eV, slightly smaller than the 4.44 eV calculated for the single crystal at A (see above). The binding energies of the

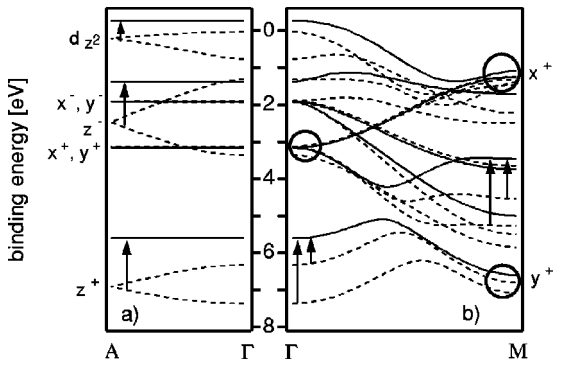

FIG. 5. Comparison of calculated band structures of single crystal (dashed lines) and single layer (solid lines) WS_2 along ΓA (a) and ΓM (b). The single layer binding energies are rigidly shifted upwards by -0.31 eV so that their x^+ and x^- states at Γ have almost identical binding energies than those of the single crystal. In (b) the extremal values of the x^+ and y^+ orbital combinations at Γ and M are indicated by circles. Arrows indicate the shift of the z states of the single layer compared to the single crystal states.

x^+ and x^- combinations at Γ are 3.46 and 2.22 eV giving a difference of 1.24 eV. This is almost the same as the 1.21 eV difference at A calculated for the single crystal band structure.

C. Comparison of calculated band structures

As mentioned above, the intralayer bonding combinations of the S p_x and p_y orbitals (x^+ and y^+) are degenerate at Γ. This degeneracy is lifted when $\mathbf{k}$ has a component in the xy plane. In the ΓM $(=\Sigma)$ direction, e.g., which is parallel to the y axis, the p_x band disperses upwards (to lower binding energies) with increasing $\mathbf{k}$, while the p_y band disperses downwards. For the single crystal the p_x and p_y bands both show a small splitting into pairs of bands along Σ because of the interlayer interaction. At the M point of the Brillouin zone the difference in binding energy between the p_x and p_y bands amounts to almost 6 eV (see Fig. 5). The downward dispersion of the p_y band is not readily identified in Figs. 3 and 4, since they hybridize between Γ and M with the upward dispersing z^+ bands.

For a better comparison the calculated single layer and single crystal band structures along ΓA and ΓM are shown together in Fig. 5. In this figure the single layer data are shifted upwards in energy so that the x^+ and x^- bands at Γ for single layer and single crystal yield similar binding energies. Such a rigid binding energy shift for a comparison of the two band structures is reasonable since interlayer interactions will have only a small effect on the x and y states. This is further confirmed by the almost identical band width of the S $3p$ x^+ and y^+ bands, which is indicated by the circles in Fig. 5(b).

Despite all similarities there is a striking discrepancy between the two band structures. When the binding energies of the single layer states are shifted so that x^+ and x^- states are in accordance with the corresponding single crystal energies as done in Fig. 5, the S $3p$ z^+ and z^- states of the single layer have more than 1 eV lower binding energies at Γ compared to the single crystal states. This is indicated by the arrows in Fig. 5(a). A somewhat smaller but corresponding difference is observed for the W $5d_{z^2}$ states. These shifts are not restricted to the Γ point but are present in the same magnitude throughout the whole Brillouin zone as indicated, e.g., for the Σ direction in Fig. 5(b).

While the calculated band widths and dispersions of the energy states are very similar for both single layer and single crystal, the electronic states derived from z-like orbitals have a lower binding energy in the single layer. We attribute this to the missing interlayer interactions, which are expected to affect these states. This result, which is theoretically predicted from the presented band structure calculations, is not observed experimentally as described in the following section.

The differences in single crystal and single layer band structure cannot directly be compared to the two available band structure calculations, because TiS_2 (Ref. 4) has a different crystal structure compared to WS_2. On the other hand a different wave function basis has been used in the calculation for MoS_2 single crystal and single layer.[10,29] The effect of the wave function basis can therefore not clearly be distinguished from the change of dimension in the latter work.

IV. EXPERIMENTAL BAND STRUCTURES

A. Experimental setup

The valence band structures were determined using angle-resolved photoelectron spectroscopy with synchrotron radiation as excitation source. A commercial VG ADES 500 spectrometer was attached to the TGM 7 beamline of the BESSY I storage ring in Berlin, Germany. The system is equipped with an angle resolving electron spectrometer mounted on a two-axis goniometer and a rear-view low energy electron diffraction (LEED) optics. The analyzer pass energy was set to 15 eV giving an experimental resolution of $\Delta E \leqslant 200$ meV for excitation energies $h\nu \leqslant 40$ eV. The angle of incidence of the incoming photons was set to 45° with respect to the surface normal. Photon energies between $h\nu = 16-80$ eV from a single monochromator grating have been used. Binding energies were calibrated by means of the Fermi cutoff of a metallic sample and intensities were normalized with respect to the photoemission current of the Au coated focussing mirror of the beamline.

The takeoff angle corresponding to normal emission of electrons is verified using the white light of synchrotron radiation reflected from the surface. To determine the angular dependence of the valence band structure the crystal was oriented using LEED to measure the emission along the high symmetry directions ΓM and ΓK. Two different angular geometries where used making use of the linear polarization of the synchrotron radiation at the beamline. *In-plane* polarization is obtained when the analyzer is rotated horizontally—in the plane of polarization of the synchrotron light. *Out-of-plane* polarization is achieved when the analyzer is rotated vertically—perpendicular to the polarization plane. This results in different selection rules for photoemission and can be used for identification of band symmetries (see, e.g., Refs. 52,53).

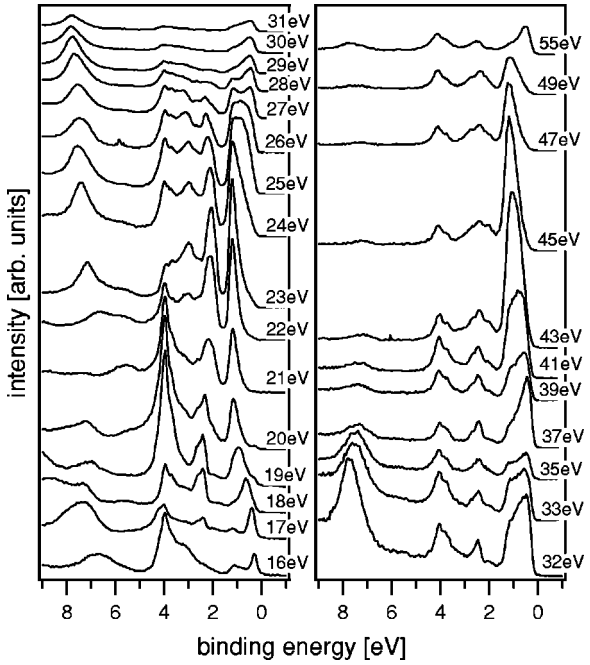

FIG. 6. Valence band photoelectron spectra of single crystal WS_2 taken in normal emission. Excitation energies are indicated.

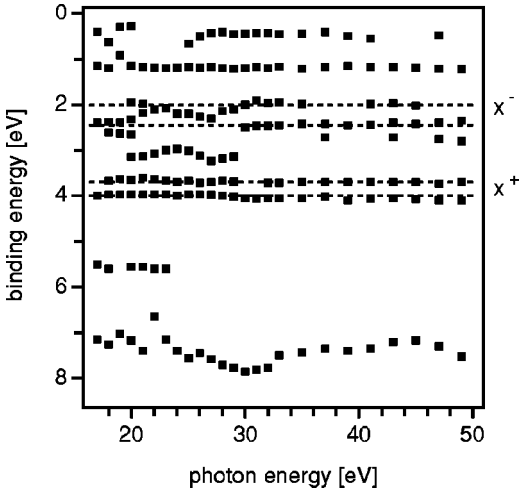

FIG. 7. Binding energies of valence band emissions of the data shown in Fig. 6. The horizontal dashed lines indicate tentatively attributed binding energies of the spin-orbit split pairs of the x^+ (3.7 and 4.0 eV) and x^- (2.0 and 2.45 eV) states, respectively.

B. Single crystal WS_2

1. Photoemission results

A WS_2 single crystal grown by chemical vapor transport with dimensions $5\times5\times0.01$ mm was fixed on the sample holder by Ag epoxy and dried at 100 °C for 1 h. The sample was cleaved in ultrahigh vacuum ($p<2\times10^{-10}$ mbar). A mirrorlike cleavage plane exhibiting a high quality hexagonal LEED pattern was obtained.

In Fig. 6 we show normal emission valence band spectra in dependence on photon energy, probing the dispersion of electronic states along ΓA. The binding energies of the photoemission peaks as determined from Fig. 6 are shown in Fig. 7.

The observed photon energy dependence is very similar to published results for $MoSe_2$,[11,17] WSe_2,[12,13] MoS_2,[15] and $MoTe_2$.[18] There are a number of nondispersing states along ΓA, which correspond to the quasi-two-dimensional structure of layered transition metal dichalcogenides. In particular, two pairs of spin-orbit split states, corresponding to the x^+ and x^- combinations of S $3p$ orbitals hybridized with W $5d$ orbitals, are expected.[54] One of these pairs can be clearly identified at binding energies BE=4.0 and 3.7 eV (see Fig. 7) giving a spin-orbit splitting of $\Delta E_{so}=0.3$ eV. An identical value has been determined for the isoelectronic WSe_2 by spin-resolved photoemission.[54] The second pair is less evident from the data. We have tentatively attributed the energetic positions of the spin-orbit split x^- bands to binding energies of 2.0 and 2.45 eV, as indicated by dashed lines in Fig. 7. Again the value of $\Delta E_{so}=0.45$ eV for the spin-orbit splitting is in good agreement with the spin-resolved data for WSe_2 by Yu *et al.*[54] The difference between the average binding energies of the x^+ and x^- states is hence given by 1.62 eV compared to the calculated value of 1.21 eV, which is a reasonable agreement.

There is another transition at a constant binding energy BE=1.1 eV, which exhibits drastic changes in intensity with varying photon energy (see Fig. 6). This band is not reflected in the band structure calculations shown in Fig. 3. Corresponding transitions are also found for other layered transition metal dichalcogenides, which also have no correspondence in the calculated band structures (see Refs. 11–13,15,17, and references therein). The photon energy dependence of this peak for $MoSe_2$ clearly indicated that this peak is predominantly of Mo $4d$ character.[11] The corresponding transition observed for single crystal WS_2 (Fig. 6) shows two intensity maxima for excitation energies around 23 and 43 eV, respectively. Almost identical intensity variations are observed for a valence band emission at 1.5 eV binding energy from single layer WS_2 [see Fig. 11(b) below]. For the single layer this transition clearly corresponds to emission from the topmost valence states at Γ, which are composed mainly from W $5d_{z^2}$ orbitals (see Sec. IV C). The dispersionless single crystal transition develops directly from the single layer W $5d_{z^2}$ state with increasing film thickness[55] [see also Fig. 11(a)]. It is therefore clearly a feature which is present already in a single layer and does not depend on three-dimensional band formation.

Different explanations for the dispersionless peak are discussed by Coehoorn *et al.*[11] Self-intercalation has been considered unlikely for $MoSe_2$,[11] which is also assumed for WS_2. Localization of d electrons due interaction with the lattice (vibronic polaron) is one of the possible explanations.[56] Dispersionless features in normal photoemission might also occur for surface states or surface resonances. However, layered transition metal dichalcogenides are generally considered as free of surface states because of the weak interlayer interactions. No clear evidence for photoemission from surface states of layered transition metal dichalcogenides exists so far (see, e.g., Ref. 57). Neverthe-

less to attribute the mentioned transition to a surface state seems to be reasonable because the W $5d_{z^2}$ orbital in the surface layer can only bond to the second layer S p_z and therefore is characterized by a nonbulk-like coordination leading to an electronic state localized at the surface. For WSe_2 this experimentally observed state may be situated within an energy gap along ΓA as suggested by the calculation presented by Traving *et al.*[12] The binding energy of the transition observed for WS_2 approximately coincides with the calculated binding energy of the interlayer antibonding z^- state (Γ_2^-). This lies between the interlayer bonding Γ_1^+ and antibonding Γ_4^- d_{z^2} states, which can be expected as the binding energy of an eventual nonbonding d_{z^2} surface state. A dangling bondlike d_{z^2} surface state would agree with the observed evolution of the d_{z^2} state with film thickness.[55]

The lowest binding energy BE$=0.29$ eV for all transitions in normal emission is observed at $h\nu=16$ eV. With increasing photon energy the binding energy of this transition increases to BE$=1.1$ eV. Further increasing $h\nu$ leads again to a backshift of its maximum to lower binding energy. However, the minimum binding energy reached at $h\nu \geqslant 30$ eV is BE$=0.42$ eV, which is significantly larger than the binding energy at $h\nu=16$ eV. A similar behavior has also been reported for WSe_2 (Ref. 12) as well as for VSe_2 and TiS_2[58]. Strocov *et al.* have attributed this behavior to increased broadening of the photoemission final state at higher kinetic energies. This leads to an asymmetrical broadening of the photoelectron peak at critical points of the occupied band structure (in-band shifting). This effect will definitely affect the observed behavior of the WS_2 valence band maximum, but we would like to mention an additional effect mentioned in the paper of Strocov *et al.*, which might be of importance in the present case. Since the surface sensitivity of the photoemission experiment changes drastically at low kinetic energies, the shift of the valence band maximum binding energy can be caused by a surface induced initial state effect. A lower binding energy of the topmost valence band observed at lower kinetic energy would correspond to a larger energy gap at the surface. This would be in agreement with the larger band gaps of single layers, which are observed for TiS_2,[4] InSe,[36] and WS_2 (see below).

Photoelectron spectra in dependence of electron emission angle were taken at photon energies $h\nu=16$ and $h\nu=21$ eV, respectively. Spectra taken with $h\nu=21$ eV are shown in Fig. 8. Pronounced binding energy shifts and intensity variations are clearly identified. The topmost filled valence band, which is composed mainly of the W d_{z^2} orbitals at Γ, disperses to higher binding energies with increasing emission angle θ. At $\theta=25°$ along ΓK [Fig. 8(b)] the peak splits into two peaks and disperses upwards to lower binding energies with increasing emission angle. At the K point of the Brillouin zone, corresponding to $\theta=45°$, the splitting of the two topmost valence band is given by $\Delta E_{so}=0.48$ eV. The splitting is again due to spin-orbit interactions and agrees with the value for WSe_2. It is significantly larger than for the molybdenum dichalcogenides[11] as can be expected from the higher ordinal of W compared to Mo. The corresponding energy states are mainly derived from $d_{x^2-y^2}$ and d_{xy} orbitals.[9,11]

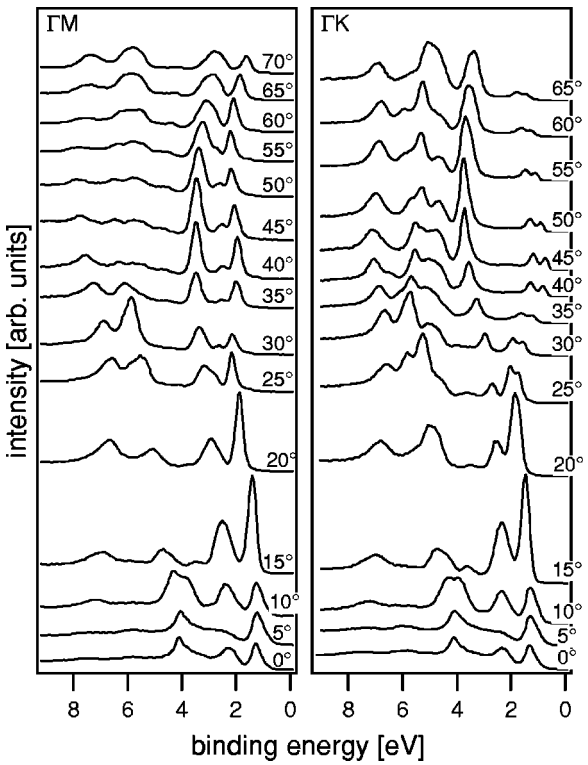

FIG. 8. Valence band spectra excited with $h\nu=21$ eV synchrotron radiation along the ΓM and ΓK direction of a $2H$-WS_2 single crystal for in-plane polarization geometry. Take off angles of photoelectrons are given on the right.

The lowest binding energy for any off-normal emissions is found at the K point with BE$=0.72$ eV. This value is 0.49 eV larger than the lowest binding energy obtained along ΓA. The experimentally determined valence band maximum of single crystal WS_2 is thus at the Γ point of the Brillouin zone, in agreement with the band structure calculation.

2. Comparison with theory

A comparison of experimental and calculated band structures of single crystal WS_2 along the high symmetry directions ΓM and ΓK is shown in Fig. 9. Except for the bands at the valence band maximum at Γ the experimental data taken with 16 eV ($\triangle$) and 21 eV ($\bigcirc$) excitation energy gave very similar binding energies. This is of course the result of the small energy dispersion perpendicular to the layers.

The experimentally observed band at Γ with BE $=5.4$ eV has no correspondence in the calculation. At this binding energy there are a number of bands both at K and M. In addition the observed transition has a rather low intensity (Fig. 8). This band is therefore most likely due to indirect transitions.

The two bands with lowest binding energy at Γ in Fig. 9 are the extremal values of the $\mathbf{k}_\perp$ dispersion of the z^+ band. These values are well reproduced by experiment (see Fig. 6). In Fig. 9 there is only one experimental band at this binding energy, as only data for a single excitation energy are shown.

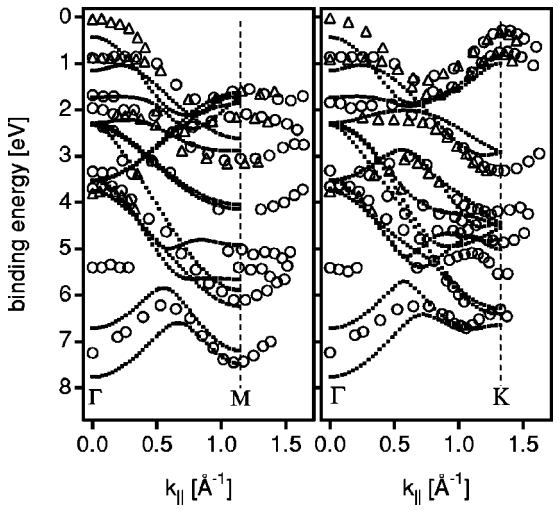

FIG. 9. Experimental and theoretical valence band structure of WS_2 single crystal. Experimental data are shown for in plane polarization and $h\nu=21$ eV (○) and $h\nu=16$ eV (△). The experimentally determined valence band maximum is set to 0 eV binding energy. Calculated bands are shifted in energy to best match the experimental data.

The agreement between experimental and calculated band structure is very good. The valence band maximum is consistently found at the Γ point of the Brillouin zone. Throughout the Brillouin zone experiment and theory do also agree with respect to the relative binding energies of the bands derived from orbitals in the basal plane (x^+ and x^- bands) and the bands derived from orbitals perpendicular to the planes. In addition the experimentally determined bandwidth of the x^+ band, which has been discussed in Sec. III C [see Fig. 5(b)], is quite well reproduced by our calculation.

C. Single layer WS_2

1. Thin film growth

Thin films of WS_2 were grown by metal-organic van der Waals epitaxy (MOVDWE) using $W(CO)_6$ and S_n as precursors.[38,39] The partial pressures, which are crucial for successful film deposition, were monitored using a mass spectrometer during deposition. Deposition was performed in a home made deposition chamber with a base pressure below 10^{-9} mbar, which was connected to the spectrometer vacuum system allowing for direct sample transfer between film deposition and analysis. Single crystalline graphite substrates have been cleaved in air and clamped to a molybdenum sample holder. A clean surface was obtained after heating in vacuum to $T>800\,^{\circ}$C for 30 min at pressures $p<10^{-8}$ mbar. The quality of the surface was checked with LEED and valence band photoemission.

The low deposition rate in MOVDWE, 2 h of deposition correspond to approximately one monolayer, has been related to the missing bonding sites of the precursor molecules on the van der Waals plane.[39] Epitaxial growth of the WS_2 film follows from the LEED patterns which are shown in Fig. 10. A clear hexagon is observed for the graphite substrate. With increasing deposition time the graphite spots are

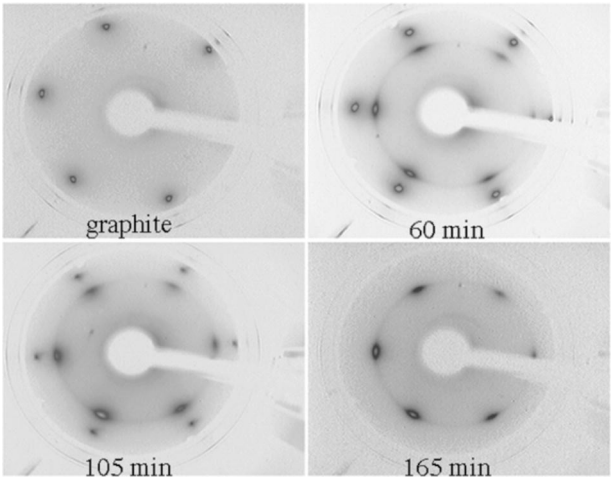

FIG. 10. LEED pattern for single crystal graphite and with increasing WS_2 film thickness ($E_{kin}=72$ eV). Deposition times are indicated. The contrast is strongly enhanced to emphasize the residual ringlike diffraction feature of the growing film.

gradually replaced by the WS_2 diffraction pattern, which mainly appears as a hexagonal mesh aligned to the graphite spots. Applying strong contrast enhancement to the LEED pattern a partial misalignment of the WS_2 film to the graphite substrate can be identified from the ringlike pattern at diffraction angles corresponding to the growing overlayer lattice constant (see Fig. 10). However, for nonoptimized deposition conditions only a ringlike diffraction pattern is obtained for the overlayer.

We have evaluated the LEED intensities along two different diagonal lines in the pattern obtained after 60 min of WS_2 deposition. The ratio of the distance between opposite spots of graphite and WS_2 is $1.25(\pm 0.01)$ for both lines. In contrast the ratio between the WS_2 and the graphite bulk lattice constants from literature data is $3.153/2.46=1.28$. This difference indicates a 2.5% smaller in-plane (a) lattice constant for the single layer WS_2 compared to the single crystal. However, the difference might also be within the general uncertainty of the LEED experiment and the uncertainty of the WS_2 bulk lattice constant.

2. Photoemission results

In Fig. 11(a) we show valence band photoelectron spectra excited with $h\nu=16$ eV as a function of deposition time. For low coverage there are two strong and one weak emission at binding energies of 1.5, 4.2, and 3 eV, respectively. The binding energy of the peak at 1.5 eV (labeled Γ_1^+ in Fig. 11) is independent on coverage. For increasing coverage a new peak appears at lower binding energies (Γ_4^-). This observation is in agreement with previous measurements on InSe grown on pyrolytic graphite.[36] The occurrence of the Γ_4^- emission indicates the growth of the second layer as the splitting of the topmost level is due to the interlayer interactions (see also Fig. 2). For deposition times of one hour or less the Γ_4^- emission is absent. We therefore assume that only islands of single layer thickness are present for these coverages.

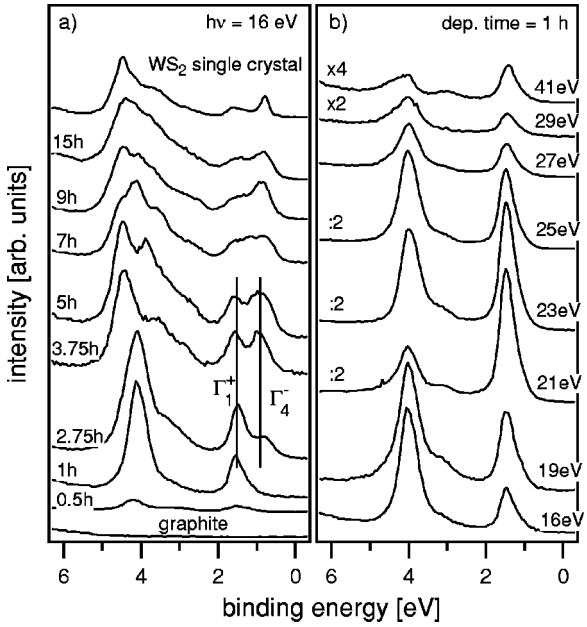

FIG. 11. (a) Valence band photoelectron spectra taken with $h\nu = 16$ eV for films of increasing thickness. The deposition times are indicated on the left. Spectra are normalized to the incoming photon flux. (b) Photon energy dependence of normal emission valence band spectra for WS_2 after 1 h of deposition.

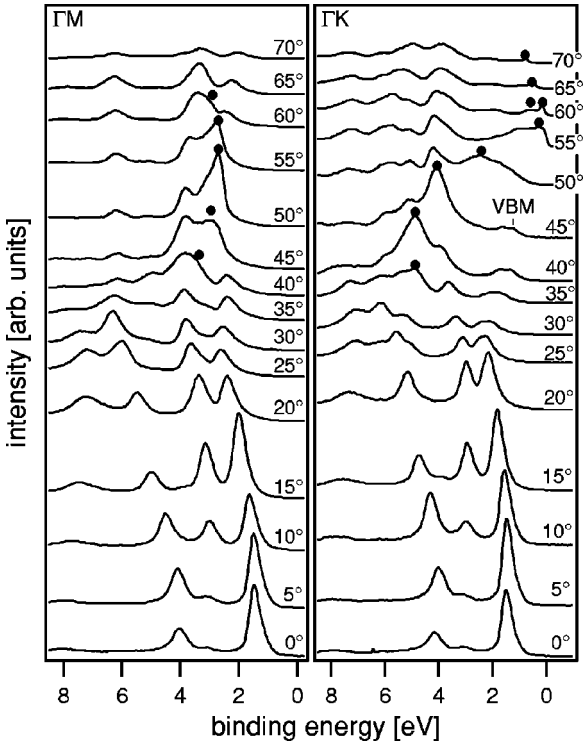

FIG. 12. Valence band spectra of thin film WS_2 deposited on single crystal graphite after 1 h of deposition. The spectra are taken with $h\nu = 21$ eV excitation energy along the ΓM and ΓK direction. Takeoff angles of photoelectrons are given on the right. Emissions from the graphite substrate are indicated by solid circles. The valence band maximum of the film is observed at 45° takeoff angle along Γ K.

The observation of the transition from single layer to double layer coverage further indicates that the WS_2 films are electronically nearly decoupled from the graphite substrate in agreement with the observation on the InSe films.[36] One can therefore assume that the valence band structures determined from the deposited WS_2 films are not strongly disturbed by the substrate. The two-dimensional nature of the electronic structure of the deposited film is further proven by the energy independent binding energies of the transitions in normal emission, which is shown for the single layer film in Fig. 11(b).

Angular dependent valence band spectra taken from the single layer film with $h\nu = 21$ eV are shown in Fig. 12. The spectra were taken along the ΓM and ΓK symmetry lines with in-plane detection geometry. Emissions from the graphite substrate are not completely attenuated for this film thickness at all emission angles and are indicated by solid circles.

The emissions from the WS_2 layer are clearly visible as a result of the strong photoionization cross sections of the contributing W $5d$ and S $3p$ levels.[59] They dominate for most emission angles those from the graphite substrate. Transition from the graphite substrate at this photon energy are not observed for most emission angles.[60] The sharp structures of the WS_2 emission indicate well-defined transitions in **k** space and allow accurate binding energy determination.

The binding energy of the topmost energy level in normal emission is 1.5 eV [Figs. 11(b)], while along ΓK the lowest binding energy for film derived emissions is 1.2 eV observed at takeoff angle 45° (Fig. 12). Hence, in contrast to the WS_2 single crystal (Sec. IV B) and also in contrast to the band structure calculation for the single layer (Sec. III B), the valence band maximum for the single layer film is experimentally found at the K point of the Brillouin zone. The valence band maximum of single layer WS_2 is hence mostly composed of the spin-orbit split $d_{x^2-y^2}$ and d_{xy} orbitals.[11]

3. Comparison with theory

The experimental valence band structure of the single layer WS_2 along ΓM and ΓK is derived from the data shown in Fig. 12 and from additional data which are taken with $h\nu = 21$ eV in out-of-plane detection geometry. The resulting band structure is shown in Fig. 13 together with the calculated band structure. Data from in-plane geometry are shown as open circles while data from out-of-plane geometry are shown as open triangles. Symmetry labels for the calculated bands are indicated for Γ and M.

It is remembered that the general difficulty of photoemission experiments to determine the absolute value of **k** inside the substrate (see, e.g., Refs. 52,53) does not affect the data in Fig. 13. The perpendicular component of **k** in monolayers is always zero. One can therefore expect a direct one-to-one correspondence of experimental and theoretical band structures. But the agreement between experiment and theory for the single layer shown in Fig. 13 is less good than the agreement found for the single crystal (see Fig. 9). To understand the differences observed between experiment and theory in more detail it is helpful to identify the symmetry of the experimental bands. With this knowledge individual experi-

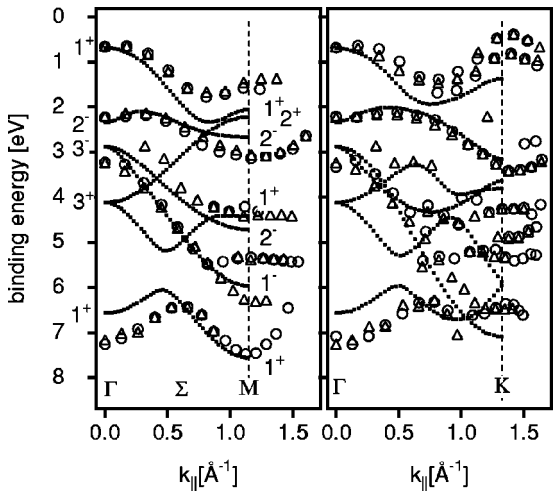

FIG. 13. Experimental and theoretical valence band structure of a WS_2 single layer. Experimental data are shown for $h\nu=21$ eV with in-plane (○) and out-of-plane (△) detection geometry. The experimental values are shifted to the same binding energies as in Fig. 14. Calculated bands are rigidly shifted in energy to give best agreement with the experimental data.

mental bands can be directly attributed to certain theoretical bands for a direct comparison of critical point energies.

Because of missing data in the literature we have evaluated the photoemission selection rules for emission along the Σ direction for the single layer. With the selection rules the point group symmetry of the single layer can be checked. If there is significant interaction of the layer with the substrate then the symmetry of the layer should be reduced giving rise to increased hybridization (see, e.g., Ref. 61).

The appropriate point group for the Σ direction of single layer WS_2 is $Pmm2$ (C_{2v}^1). No change of symmetry occurs when the *M* point is reached. The symmetry labels given in Fig. 13 for the *M* point are therefore also appropriate for the Σ line. The corresponding character table for $Pmm2$ is shown in Table I. For convenience the orientation of the crystallographic axis is the same as for the crystal so that *y* corresponds to the twofold rotational axis of $Pmm2$. In standard character tables of C_{2v} the directions *y* and *z* are exchanged compared to Table I. There are four one-dimensional irreducible representations Σ_1^+, Σ_1^-, Σ_2^+, and Σ_2^-, where the notation of Bassani *et al.*[3] and of Bromley *et al.*[7] is adopted. The superscripts + and − denote even and odd symmetry with respect to reflection at the basal *xy* plane.

TABLE I. Character table for the Σ direction of the hexagonal Brillouin zone (point group $Pmm2$). The axes and symmetry operations are labeled according to the $P\bar{6}m2$ space group resulting in $y\|\Sigma$ and the symmetry operations E (identity), C_2 (twofold rotation along *y*), σ_h (reflection at *xy*), and σ_v (reflection at *yz*), respectively.

		Σ [a]	Σ [b]	E	C_2	σ_h	σ_v
z^2, x^2-y^2	*y*	1^+	1	1	1	1	1
xz		1^-	2	1	1	−1	−1
xy	*x*	2^+	4	1	−1	1	−1
yz	*z*	2^-	3	1	−1	−1	1

[a]Symmetry labels according to Refs. 7,3.
[b]Symmetry labels according to Ref. 62.

TABLE II. Selection rules for photoemission along the Σ direction for polarization along the three principal axes ($y\|\Sigma$). In-plane polarization gives components of the electric field vector $\vec{E}\|y$ and $\vec{E}\|z$, out-of-plane polarization gives $\vec{E}\|x$ and $\vec{E}\|z$.

polarization	initial state :	Σ_1^+	Σ_1^-	Σ_2^+	Σ_2^-
$\vec{E}\|x$	final state :	Σ_2^+	Σ_2^-	Σ_1^+	Σ_1^-
$\vec{E}\|y$	final state :	Σ_1^+	Σ_1^-	Σ_2^+	Σ_2^-
$\vec{E}\|z$	final state :	Σ_2^-	Σ_2^+	Σ_1^-	Σ_1^+

The selection rules for direct optical transitions along Σ are presented in Table II for light polarized along *x*, *y*, and *z*, respectively. In our experimental setup in-plane polarization corresponds to light polarized in the *yz* plane with equal contributions along *y* and *z*, and out-of-plane polarization corresponds to light polarized in *xz* plane with equal contributions along *x* and *z*.

Since the Σ direction, which is parallel to *y*, lies in the *yz* mirror plane, the photoemission final state must have even symmetry with respect to σ_v. Otherwise zero intensity at the detector is obtained.[52,53] Therefore only Σ_1^+ and Σ_2^- final states are allowed. Table III lists the allowed transitions for both measurement geometries. Using in-plane polarization, only transitions from Σ_1^+ and Σ_2^- initial states are allowed, while transitions from all initial states are allowed for out-of-plane polarization. With the knowledge of the allowed transitions we have identified unambiguously the symmetries of the experimentally observed transitions, which are also tabulated in Table III. The transition around 6 eV at *M*, e.g., (see Fig. 13), is obviously related to the Σ_1^- band, as it is observed for out-of-plane polarization only.

In contrast to Table III, the Σ_2^+ band, starting at Γ_3^+ and dispersing upwards towards M_2^+ (see Fig. 13), is not observed for any of the two polarizations. Photoemission from the corresponding single crystal band is only observed for larger emission angles with weak intensity between two stronger emissions (compare Figs. 8 and 9). The two stronger emissions are also observed for the single layer and are due to transitions from the neighboring M_1^+ and M_2^- bands. We therefore assume that the Σ_2^+ band is not observed for the single layer because of a low photoionization cross section. To support this assumption we have calculated angular de-

TABLE III. Allowed and observed transitions for photoemission of single layer WS_2 along Σ for light polarization in the emission plane and perpendicular to it.

	allowed	observed
in-plane	Σ_1^+, Σ_2^-	Σ_1^+, Σ_2^-
out-of-plane	Σ_1^+, Σ_1^-, Σ_2^+, Σ_2^-	Σ_1^+, Σ_1^-, Σ_2^-

TABLE IV. Calculated and experimental binding energies of critical points Γ and M of single layer WS_2. Experimental values are given with an uncertainty of $\leqslant 0.1$ eV for comparison where available. The binding energies are given in eV with respect to the topmost band at Γ.

	Γ_1^+	Γ_2^-	Γ_3^-	Γ_3^+	Γ_1^+		
theory	0	1.65	2.18	3.43	5.88		
experiment	0	1.57		2.58	6.56		
	M_1^+	M_2^+	M_2^-	M_1^+	M_2^-	M_1^-	M_1^+
theory	1.36	1.52	1.98	3.73	4.02	5.27	6.86
experiment	0.87		2.42	4.70	3.68	5.65	6.82

pendent photoionization cross sections using the theory for atomic orbitals with fixed orientation presented by Goldberg *et al.*[63] The Σ_2^+ band is composed from d_{xy} and from x^+ combinations of the S $3p$ orbitals. Our calculation predicts a considerably lower transition probability for emission from the d_{xy} orbitals than for the other d orbitals in the respective emission direction y, in agreement with the above assumption.

Angular variations of photoionization cross sections are also suggested to be responsible for low emission intensities of the lower Σ_2^- band, which starts at Γ_3^- dispersing downwards towards M_2^-. Although this band seems to agree excellently with experimental transitions, the corresponding data points are due to the transition from the Σ_1^+ band, which starts at Γ_3^+ dispersing downwards. This band hybridizes halfway between Γ and M with the upward dispersing band from the bottom most Γ_1^+ band. The lower Σ_2^- corresponds to the data points which are observed for in-plane polarization only around the M point. Transitions at lower emissions angles are observed for out-of-plane polarization only. These findings are in agreement with cross section calculations using d_{yz} orbitals.

The observed photoemission selection rules are thus fully consistent with those expected for the $Pmm2$ point group, at least for the ΓM direction. It is, however, assumed that the agreement between experiment and the full symmetry for the single layer also holds for the other directions. Any residual electronic interactions with the substrate, which should reduce the symmetry, can therefore be considered as very small.

With the one-to-one correspondence of theoretical and experimental bands it is now possible to compare the experimentally determined critical point energies with those predicted by the band structure calculations. The result is shown in Table IV where binding energies are given in eV with respect to the topmost band at Γ.

Reasonable agreement between experimental and theoretical values at Γ is found for the upper 1^+ and the 2^- state. The lower 1^+ state (z^+) and the 3^+ (x^+) and 3^- (x^-) states show larger discrepancies. At the M point reasonable agreement is obtained for the lower 1^+, the 1^- and the two 2^- states. Rather poor agreement is achieved for the other states. The too low binding energy of the calculated topmost M_1^+ state corresponds to the observation for the topmost band at K. The deviation at this point leads to a different location of the valence band maximum in **k** space as determined by band structure calculation and experiment.

A possible explanation for the differences between theoretical and experimental band structures of single layer WS_2 is the relaxation of the crystal structure. In the calculations we have assumed identical atomic positions for single layer and single crystal within the slab since no detailed crystallographic data are available for the single layer. As mentioned above the LEED pattern obtained for single layer indicates a 2.5% smaller in-plane lattice constant. Further hints for a different lattice constant of the single layer give the experimentally determined band structure. Some of the bands have maxima or minima at the corner of the Brillouin zone. The **k** values of the M and K points as expected from the bulk lattice constant are indicated by the vertical dashed lines in Fig. 13. The extrema of the upper Σ_2^- band and of the two topmost bands around K are clearly observed at **k** values which are larger than the expected position. By fitting parabolic functions to the extrema of these bands a decrease of the lattice constant for single layer WS_2 of 5% compared to the bulk lattice constant is deduced. However, the estimated uncertainty of this value is rather high and no deviation from the lattice constant is observed from other extrema at the M point. In addition we would expect a decrease of the in-plane lattice constant of 5% to increase the band width of the x^+ band. In contrast the experimentally determined band widths are very similar for single crystal and single layer as described in the next section. Therefore no convincing experimental evidence for a relaxation of the single layer can be extracted.

4. Comparison with single crystal band structure

The experimental valence band structures of single crystal and single layer WS_2 along ΓM and ΓK are compared in Fig. 14. Open symbols show dispersion of energy bands for single crystal WS_2 obtained with photon energies $h\nu = 21$ eV (circles) and $h\nu = 16$ eV (triangles). Data from scans with out-of-plane polarization are omitted. Filled symbols show dispersion of energy bands for the WS_2 film after 1 h of deposition obtained with $h\nu = 21$ eV and in-plane polarization (circles) and out-of-plane polarization (triangles), respectively. The binding energy of the valence band maximum of the single crystal band structure is set to 0 eV, while the band structure of the single layer is shifted in energy to best match the single crystal data.

The most striking differences between the single crystal and the single layer band structure are some additional bands observed for the single crystal. These are the splitting of the topmost valence band at Γ and the occurrence of emissions at binding energies of 5.5 eV around Γ and of $2-2.5$ eV around M. The splitting of the topmost valence band is due to interlayer interaction, which has been discussed above and in Ref. 36. Indirect transitions from regions of high density of states are assumed to account for the nondispersing band at 5.5 eV close to Γ as discussed in Sec. IV B 1. The band at the M point is most likely not observed for the single layer due to low photoionization cross sections as discussed in the previous section.

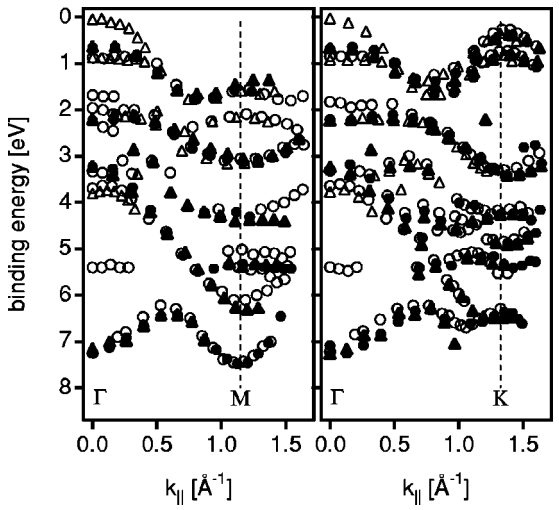

FIG. 14. Experimental valence band structures of WS_2 along the ΓM- and ΓK directions: Single crystal, in plane polarization: $h\nu = 21$ eV (○), $h\nu = 16$ eV (△). Single layer, $h\nu = 21$ eV: in plane polarization (●), out of plane polarization $h\nu = 16$ eV (▲). The valence band maximum of the single crystal is set to 0 eV. The single layer bands are shifted in energy to best match the single crystal data. Symmetry labels are indicated for the calculated energy bands at Γ and M.

Apart from these differences there is an excellent agreement between the two experimental band structures. The energy states are in very good agreement regardless of their orientation with respect to the layer structure. This is in contrast to the theoretical band structure calculations, which predict an upward shift of the z derived states relative to the x,y derived states for the single layer (see Sec. III C).

The origin of this discrepancy between experimental and theoretical data is not clear yet. One might, e.g., assume residual bonding interactions of the single layer film with the graphite substrate. However, the results in Sec. IV C 3 indicate that the film is almost completely electronically decoupled from the substrate as it exhibits the symmetry properties of a nonsupported film. The electronic coupling of overlayer and substrate is inhibited by the large differences in electronic and crystallographic structure.[21,36] Strong modifications of the single layer band structure by substrate interactions are therefore not expected.

Another explanation could be that with photoemission only the top layer of the single crystal is probed, which might have an electronic structure significantly different from the bulk. This effect has been discussed by Fang *et al.*[4] However, for the single crystal a much better agreement between experimental and theoretical band structure is observed than for the single layer. Hence the electronic structure of the single layer, which should be comparable to the electronic structure of the surface within this argumentation, is less well predicted by theory. In addition, the splitting of the topmost valence band, which is always observed with photoemission from single crystal Mo and W dichalcogenides, is a clear indication of interlayer interactions. Photoemission of single crystalline layered materials will therefore mainly probe the bulk electronic structure.

The most convincing explanation for the dissimilarity of experimental and theoretical results is the assumption of a structural relaxation of the single layer. There are some hints for a slightly reduced in-plane lattice constant of the single layer from LEED and angle resolved photoemission (see Sec. IV C 3). In addition, relaxation of the layer height may be expected. A detailed analysis of energy dependent LEED intensities curves, which are not available yet, would be necessary to verify this assumption.[64] For single crystal surfaces of some layered materials relaxation of the c lattice constant has been observed by LEED analysis.[65–67] For MoS_2 a contraction of the interlayer spacing of 5% is reported.[65,66] No relaxation of the in-plane lattice constant or the layer height is observed. These results may not apply to the single layer WS_2 deposited on graphite because of the different substrate-film interactions, but show that significant relaxation of lattice constants is possible.

V. SUMMARY AND CONCLUSIONS

We have determined the electronic valence band structure of single crystal and single layer WS_2 by ASW band structure calculations based on density functional theory and angle resolved photoelectron spectroscopy using synchrotron radiation as excitation source. A crystalline single layer of WS_2 has been prepared by van der Waals epitaxy on a graphite single crystal. An electronically almost completely decoupled film is obtained as is evident from the clear observation of the transition from single layer to double layer electronic states with increasing layer thickness. The single layer film obeys photoemission selection rules which are appropriate for a nonsupported film and therefore also strongly suggests electronic decoupling. Electronic decoupling of the film is a prerequisite for the determination of an undisturbed single layer band structure.

Good agreement between experimental and theoretical band structures of single crystal WS_2 is obtained. The valence band maximum is located at the Γ point of the Brillouin zone and is derived mainly from the W $5d_{z^2}$ states. In contrast the valence band maximum of the single layer is experimentally found at the K point and is derived from d_{xy} and $d_{x^2-y^2}$ states. The different **k** position of the valence band maximum is a consequence of the missing interlayer interactions.

In normal emission an intense valence band feature, which does not disperse with photon energy, is observed for single crystal WS_2 as also reported for a large number of other transition metal dichalcogenides. Its intensity variation compares with the single layer W $5d_{z^2}$ emission. It is therefore clearly a feature which is present already in a single layer and does not depend on three-dimensional band formation. At least for materials with trigonal prismatic coordination an interpretation of the dispersionless emission as a dangling bondlike d_{z^2} surface state seems to be possible, although other explanations cannot be ruled out.

The band structure of the single layer has been calculated by assuming atomic positions derived from the crystallographic structures of bulk WS_2. With this assumption an energy shift of the z orbitals relative to the x,y orbitals com-

pared to the single crystal band structure is predicted. This is most likely related to the missing interlayer interaction of the z orbitals across the van der Waals gap. The experimental band structure of the single layer shows excellent agreement with the single crystal data for both z and x,y derived electronic states. Relaxation of the single layer atomic structure is supposed to account for this discrepancy between experimental and theoretical comparison between the two band structures. The differences can, however, also be induced by the graphite substrate. Detailed theoretical calculations might clarify this open question.

The suggested relaxation of the single layer should result in almost identical electronic structures of the single layer and the single crystal as observed experimentally. This electronic structure obviously is the energetic minimum of WS_2 and can be approached with and without interlayer interactions. Any calculations of electronic structures of single layer films or nanostructures, which assume atomic positions derived from bulk crystallographic structures, might therefore not agree with experiment. To clarify this important restriction it is planned to investigate the effect of relaxation on the band structures of single layer materials. With such calculations additional insight into the details of the interlayer interactions in layered chalcogenides are expected.

Relaxation of layered chalcogenides is also important at surfaces of layered materials. The available experimental data on such effects are very limited and show only a small but noticeable effect.[65–67] However, the interactions of the surface with the underlying bulk of the same composition are expected to be comparatively strong, because electronic coupling is possible due to at least very similar electronic and crystallographic structures. We anticipate from the results presented here that any relaxation of the surface will reduce the differences between the surface and the bulk electronic structure for layered materials. The interpretation of photoemission data in terms of bulk electronic states will then be less affected.

The question of relaxation and the details of the interlayer interactions are of great importance for interfaces between weakly interacting dissimilar materials. A great variety of such interfaces between two layered materials or between layered and three-dimensional materials can be prepared by van der Waals epitaxy.[21] The degree of electronic coupling, and hence the influence of the interlayer interactions on the electronic properties of the prepared films and interfaces, should strongly depend on the differences between electronic and crystallographic structures.

ACKNOWLEDGMENTS

We gratefully acknowledge receipt of graphite single crystals by K. Horn (Fritz-Haber-Institut, Berlin) and of WS_2 single crystal by Th. Matthes (Hahn-Meitner-Institut, Berlin). A part of this work was supported by the Deutsche Forschungsgemeinschaft within the Sonderforschungsbereich 484 and the Forschergruppe HO955/2.

[1] J. A. Wilson and A. D. Yoffe, Adv. Phys. **18**, 193 (1969).
[2] V. Grasso, *Electronic Structure and Electronic Transitions in Layered Materials* (Reidel, Dordrecht, 1986).
[3] F. Bassani and G. Pastori Parravicini, Nuovo Cimento B **50**, 95 (1967).
[4] C. M. Fang, R. A. de Groot, and C. Haas, Phys. Rev. B **56**, 4455 (1997).
[5] D. R. Allan, A. A. Kelsey, S. J. Clark, R. J. Angel, and G. J. Ackland, Phys. Rev. B **57**, 5106 (1998).
[6] G. Seifert, H. Terrones, M. Terrones, G. Jungnickel, and T. Frauenheim, Solid State Commun. **114**, 245 (2000).
[7] R. A. Bromley, R. B. Murray, and A. D. Yoffe, J. Phys. C **5**, 738 (1972); **5**, 759 (1972).
[8] D. W. Bullett, J. Phys. C **11**, 4501 (1978).
[9] L. F. Mattheiss, Phys. Rev. B **8**, 3719 (1973).
[10] K. Kobayashi and J. Yamauchi, Phys. Rev. B **51**, 17 085 (1995).
[11] R. Coehoorn, C. Haas, J. Dijkstra, C. J. F. Flipse, R. A. de Groot, and A. Wold, Phys. Rev. B **35**, 6195 (1987); R. Coehoorn, C. Haas, and R. A. deGroot, *ibid.* **35**, 6203 (1987).
[12] M. Traving, M. Boehme, L. Kipp, M. Skibowski, F. Starrost, E. E. Krasovski, A. Perlov, and W. Schattke, Phys. Rev. B **55**, 10 392 (1997).
[13] Th. Finteis, M. Hengsberger, Th. Straub, K. Fauth, R. Claessen, P. Auer, P. Steiner, S. Hüfner, P. Blaha, M. Vögt, M. Lux-Steiner, and E. Bucher, Phys. Rev. B **55**, 10 400 (1997); **59**, 2461 (1999).
[14] R. Mamy, A. Boufelja, and B. Carricaburu, Phys. Status Solidi B **141**, 467 (1987).
[15] K. Fives, I. T. McGovern, R. McGrath, R. Cimino, G. Hughes, A. McKinley, and G. Thornton, J. Phys.: Condens. Matter **4**, 5639 (1992).
[16] P. K. Larsen, S. Chiang, and N. V. Smith, Phys. Rev. B **15**, 3200 (1977).
[17] T. Böker, Ph.D. thesis, Humboldt University, Berlin, 2000.
[18] T. Böker, A. Müller, J. Augustin, C. Janowitz, and R. Manzke, Phys. Rev. B **60**, 4675 (1999).
[19] *Electron Spectroscopies Applied to Low-dimensional Materials*, edited by H. P. Hughes and H. I. Starnberg (Kluwer Academic, Dordrecht, 2000).
[20] L. Kipp and M. Skibowski, in *Electron Spectroscopies Applied to Low-dimensional Materials* (Ref. 19), pp. 1-39.
[21] W. Jaegermann, A. Klein and C. Pettenkofer, in *Electron Spectroscopies Applied to Low-dimensional Materials* (Ref. 19), pp. 317–402.
[22] A. Koma, K. Sunouchi, and T. Miyajima, J. Vac. Sci. Technol. B **3**, 724 (1985); A. Koma, Surf. Sci. **267**, 29 (1992).
[23] R. H. Friend and A. D. Yoffe, Adv. Phys. **36**, 2 (1987).
[24] M. Balkanski, *Microionics—Solid State Integratable Batteries* (Elsevier, Brussels, 1991).
[25] H. I. Starnberg, H. E. Brauer, and H. P. Hughes, in *Electron Spectroscopies Applied to Low-dimensional Materials)* (Ref. 19), pp. 41–98.
[26] R. Tenne, L. Margulis, M. Genut, and G. Hodes, Nature (London) **360**, 444 (1992).
[27] L. Margulis, G. Salitra, R. Tenne, and M. Talianker, Nature (London) **365**, 113 (1993).

[28] E. Bucher, in *Photoelectrochemistry and Photovoltaics of Layered Semiconductors*, edited by A. Aruchamy (Kluwer Academic Publishers, Dordrecht, 1992).
[29] The absolute valence band widths of the four layer slabs are approximately 6.5 eV and 8.2 eV for the plane wave and the LCAO basis sets, respectively (Ref. 10). The different band widths can at least partly be attributed to a different binding energy separation between the electronic states derived from orbitals perpendicular and parallel to the layer structure.
[30] D. Yang, S. Jiménez Sandoval, W. M. R. Divigalpitiya, J. C. Irwin, and R. F. Frindt, Phys. Rev. B **43**, 12 053 (1991).
[31] D. Yang and R. F. Frindt, J. Phys. Chem. Solids **57**, 1113 (1996).
[32] M. A. Py and R. R. Haering, Can. J. Phys. **61**, 76 (1983).
[33] A. Schellenberger, W. Jaegermann, C. Pettenkofer, M. Kamaratos, and C. A. Papageorgopoulos, Ber. Bunsenges. Phys. Chem. **98**, 833 (1994).
[34] C. A. Papageorgopoulos and W. Jaegermann, Surf. Sci. **338**, 83 (1995).
[35] P. C. Klipstein and R. H. Friend, J. Phys. C **17**, 2713 (1984).
[36] A. Klein, O. Lang, R. Schlaf, C. Pettenkofer, and W. Jaegermann, Phys. Rev. Lett. **80**, 361 (1998).
[37] C. Kreis, M. Traving, R. Adelung, L. Kipp, and M. Skibowski, Europhys. Lett. **52**, 189 (2000).
[38] S. Tiefenbacher, H. Sehnert, C. Pettenkofer, and W. Jaegermann, Surf. Sci. Lett. **318**, L1161 (1994); S. Tiefenbacher, C. Pettenkofer, and W. Jaegermann, in *Thin Films—Structure and Morphology*, edited by S. C. Moss *et al.*, MRS Symp. Proc. No. 441 (Materials Research Society, Pittsburgh, 1997), p. 591.
[39] S. Tiefenbacher, Ph.D. thesis, Technische Universität, Berlin, 1998.
[40] J.-W. Chung, Z. R. Dai, and F. S. Ohuchi, J. Cryst. Growth **186**, 137 (1998); J.-W. Chung, Z. R. Dai, K. Adib, and F. S. Ohuchi, Thin Solid Films **335**, 106 (1998).
[41] W. J. Schutte, J. L. de Boer, and F. Jellinek, J. Solid State Chem. **70**, 207 (1987).
[42] E. Doni, R. Girlanda, V. Grasso, A. Balzarotti, and M. Piacentini, Nuovo Cimento Soc. Ital. Fis., B **51**, 154 (1979).
[43] P. Hohenberg and W. Kohn, Phys. Rev. **136**, B864 (1964).
[44] W. Kohn and L. J. Sham, Phys. Rev. **140**, A1133 (1965).
[45] A. R. Williams, J. Kübler, and C. D. Gelatt, Jr., Phys. Rev. B **19**, 6094 (1979).
[46] V. Eyert, Ph.D. thesis, Technische Hochschule Darmstadt, 1991.
[47] J. Kübler and V. Eyert, in *Electronic and Magnetic Properties of Metals and Ceramics*, edited by K. H. J. Buschow (VCH Verlagsgesellschaft, Weinheim, 1992), pp. 1–145; Volume 3A of *Materials Science and Technology*, edited by R. W. Cahn, P. Haasen, and E. J. Kramer (VCH Verlagsgesellschaft, Weinheim, 1991).
[48] V. Eyert, Int. J. Quantum Chem. **77**, 1007 (2000).
[49] O. K. Andersen, Phys. Rev. B **12**, 3060 (1975).
[50] V. Eyert and K.-H. Höck, Phys. Rev. B **57**, 12 727 (1998).
[51] V. Eyert, J. Comput. Phys. **124**, 271 (1996).
[52] S. Hüfner, *Photoelectron Spectroscopy* (Springer-Verlag, Berlin, 1995).
[53] E. W. Plummer and W. Eberhardt, Adv. Chem. Phys. **49**, 533 (1982).
[54] S.-W. Yu, T. Lischke, R. David, N. Müller, U. Heinzmann, C. Pettenkofer, A. Klein, A. Y. Perlov, E. E. Krasovskii, W. Schattke, and J. Braun, J. Electron Spectrosc. Relat. Phenom. **101-103**, 449 (1999).
[55] A. Klein, S. Tiefenbacher, C. Pettenkofer, and W. Jaegermann (unpublished).
[56] D. K. G. de Boer, C. F. van Bruggen, G. W. Bus, R. Coehoorn, C. Haas, G. A. Sawatzky, H. W. Myron, D. Norman, and H. Padmore, Phys. Rev. B **29**, 6797 (1984).
[57] E. Pehlke and W. Schattke, J. Phys. C **20**, 4437 (1987).
[58] V. N. Strocov, H. I. Starnberg, P. O. Nilsson, H. E. Brauer, and L. J. Holleboom, J. Phys.: Condens. Matter **10**, 5749 (1998).
[59] J. Yeh and I. Lindau, At. Data Nucl. Data Tables **32**, 1 (1985).
[60] A. R. Law, J. J. Berry, and H. P. Hughes, Phys. Rev. B **28**, 5332 (1983); A. R. Law, M. T. Johnson, H. P. Hughes, *ibid.* **34**, 2389 (1986).
[61] K. Jacobi, C. v. Muschwitz, and K. Kambe, Surf. Sci. **93**, 310 (1980).
[62] M. Schlüter, Nuovo Cimento Soc. Ital. Fis., B **13**, 313 (1973).
[63] S. M. Goldberg, C. S. Fadley, and S. Kono, J. Electron Spectrosc. Relat. Phenom. **21**, 285 (1981).
[64] M. A. Van Hove, W. H. Weinberg, and C.-M. Chan, *Low-Energy Electron Diffraction* (Springer-Verlag, Berlin, 1986).
[65] M. A. van Hove, S. Y. Tong, and M. H. Elconin, Surf. Sci. **64**, 85 (1977).
[66] B. J. Mrstik, R. Kaplan, T. L. Reinecke, M. Van Hove, and S. Y. Tong, Phys. Rev. B **15**, 897 (1977); Nuovo Cimento Soc. Ital. Fis., B **38**, 387 (1977).
[67] M. Kasch, E. Pehlke, W. Schattke, T. Kurberg, H. P. Barnscheidt, R. Manzke, and M. Skibowski, Surf. Sci. **214**, 436 (1989).